

Canopy height uniformity: a new 3D phenotypic indicator linking individual plant to canopy



Wushuai Chang^{a,b,1}, Weiliang Wen^{b,c,1}, Shenghao Gu^b, Yinglun Li^b, Jiangchuan Fan^b, Xianju Lu^b, Bo Chen^c, Tianjun Xu^d, Ronghuan Wang^d, Xinyu Guo^{b,c,*}, Ruiqi Li^{a,*}

^a College of Agronomy, Hebei Agricultural University, Baoding 071001, China

^b Information Technology Research Center, Beijing Academy of Agriculture and Forestry Sciences, Beijing 100097, China

^c Beijing Key Lab of Digital Plant, National Engineering Research Center for Information Technology in Agriculture, Beijing 100097, China

^d Maize Research Institute of Beijing Academy of Agricultural and Forestry Sciences, Beijing 100097, China

ARTICLE INFO

Keywords:

UAV
Lidar
Plant height
Canopy height uniformity
Above ground biomass

ABSTRACT

Canopy height uniformity (CHU) is a key indicator linking individual plants to populations. Determining CHU by the manual measurement of the height of individual plants is inefficient and subjective, making meeting the demand for a high-throughput assessment of CHU in high-yield crop management and variety selection challenging. Therefore, a high-throughput CHU estimation approach using unmanned aerial vehicle (UAV) light detection and ranging (LiDAR) data is proposed. First, individual plant point clouds were segmented by incorporating planting density, and the CHU was estimated based on the extracted plant heights (PHs). The CHU was then applied to quantify the effects of different cropping practices on maize canopy structure. In addition, 18 canopy structural parameters (SPs) were extracted from the canopy point cloud, and aboveground biomass (AGB) was estimated by combining these SPs with Pelican Optimization Algorithm (POA) machine learning models (POA-MLs). Finally, as an indicator of individual variability within the canopy, CHU was integrated into the training process to evaluate the accuracy of AGB estimation for different models and datasets. The results showed that the plant height extracted by the canopy population-individual plant segmentation was accurate, with R^2 ranging from 0.85 to 0.93. The CHU was able to accurately quantify the effects of different cropping practices on canopy structure. An increase in applied nitrogen fertilizer and irrigation could significantly contribute to an increase in CHU and the formation of a clean and homogeneous canopy structure. Meanwhile, marginal effects can be accurately quantified through PHs estimation to further quantify the intra-canopy differences. In addition, the accuracy of the AGB estimation can be effectively improved by merging SPs, PH, and CHU. In this study, we demonstrated the efficacy of CHU as a phenotypic indicator for representing differences in canopy structure, thus providing practical phenotypic identification information for breeders and field managers.

1. Introduction

Canopy uniformity is the quantitative difference between individuals within a crop canopy. This difference can be expressed in terms of morphology (e.g., plant height, spike height, stem diameter, and leaf area) and dry weight (DW). Canopy height uniformity (CHU) is an important phenotypic indicator for evaluating the plant canopy structure, and it has been shown that a higher CHU increases the light interception capacity of the crop canopy, thereby increasing biomass accumulation (Lu et al., 2017). At present, the measurement of canopy

height uniformity is primarily performed through manual sampling and measurement, which is labor-intensive, subjective, and inefficient, making investigating large-scale canopies challenging (Huang and Li, 1995; Has et al., 2008). Remote sensing, particularly unmanned aerial vehicle remote sensing (UAV-RS), is cost-effective and timely. Its flexible deployment and reliable data resolution enable the acquisition and resolution of CHU data in a high-throughput manner (Jin et al., 2020).

The estimation of individual plant height is crucial for calculating CHU and estimating above-ground biomass (AGB) (Bendig et al., 2015; Madec et al., 2017; Wang et al., 2019). Currently, two main methods for

* Corresponding authors.

E-mail addresses: guoxy73@163.com (X. Guo), li-rq69@163.com (R. Li).

¹ These authors contributed equally to the article.

estimating plant height using UAV-RS are constructing digital surface models (DSM) through photogrammetry or directly using point clouds from light detection and ranging (lidar) data (Bendig, 2015). The photogrammetric approach generates a DSM from a three-dimensional (3D) model reconstructed from Red-Green-Blue (RGB) images and the structure from the motion algorithm. The DSM includes visible ground and vegetation, with the vegetation height being obtained by subtracting from a digital terrain model acquired on bare ground without vegetation (Gilliot et al., 2021). However, to improve accuracy, this method requires a certain number of ground control points. Xie et al. (2021) estimated the heights of oilseed rape plants at different growth stages using the DSM acquired by UAVs and found that complete spatially assisted information improved the plant height estimation accuracy (Xie et al., 2021).

Compared to the RGB indirect DSM method, the lidar data involve elevation information. Thus, the direct use of lidar data to estimate plant height is widely used (Sun et al., 2017; Yuan et al., 2018). Previous studies used the aforementioned methods to obtain canopy-scale heights, with less attention paid to individual plant heights within the population. For instance, Wang et al. (2023) employed an airborne lidar to monitor maize plant height during the grain-filling stage by estimating the difference between the mean of the upper 5% and lower 5% of the point cloud data (Wang et al., 2023). Liu et al. (2024) utilized the 2nd and 100th percentiles of elevation as the lower and upper boundaries of lidar point clouds, respectively, to calculate the height of maize plants. A linear regression equation was established by obtaining wheat canopy ground and crop canopy lidar data at different elevation percentiles using the measured crop height (Jimenez-Berni et al., 2018). Current studies on monitoring crop plant height have mainly focused on evaluating accuracy at the population scale. However, when the canopy has significant individual differences due to stress, the selected height percentile may not represent the entire canopy. Thus, this study aims to explore CHU estimation using UAV lidar to quantitatively describe the heterogeneity in plant height within the canopy.

Current research on AGB estimation has focused on establishing correlations between vegetation indices (VIs) and AGB. However, the problem of VIs becoming saturated at higher coverages during the later stages of crop growth, resulting in low AGB estimates, remains unresolved, hindering the further development of this method (Prabhakara et al., 2015; Araza et al., 2022; Yue et al., 2023). Compared to two-dimensional (2D) data from vegetation index methods, active SAR and lidar technologies have the advantages of higher penetration, better 3D representation ability, and insensitivity to light (Walter et al., 2019; Jin et al., 2021), meaning 3D point-cloud data have the advantage of characterizing and estimating the AGB of field crops more accurately, and are considered a more reasonable method for measuring AGB (Li et al., 2020). The use of lidar data allows the extraction of structural parameters (SPs), such as the mean canopy height and height percentile, which can be used to improve the accuracy of AGB estimation. Thus, expanding the performance of 3D SPs for estimating AGB is necessary. Additionally, previous studies estimating AGB have primarily focused on the canopy scale without considering the impact of intra-canopy homogeneity on AGB estimation, resulting in a decrease in CHU when canopy stress occurs. Therefore, when using plant height information to estimate AGB, it is necessary to consider the CHU accounting for individual differences within the canopy.

This study proposes a method to extract individual maize plant heights based on UAV lidar data to achieve a high-throughput estimation of the CHU. Additionally, we aimed to use the CHU to quantify the effects of cultivation practices on the canopy structure of different maize cultivars, and explore the sensitivity of the CHU to variations in plant architecture and canopy structure. Finally, we evaluated the potential of combining CHU and canopy SPs to estimate AGB in maize.

2. Materials and Methods

2.1. Study area and experimental setup

This study was conducted in 2022 and 2023 in two ecoregions, Beijing, China, and Inner Mongolia, China, and contained three specific experiments (Table 1), with a control table of varietal names for Experiments 1 and 2 in Table 2 and the names of the varietals used in Experiment 3 in Supplementary Table S1. Experiment 1 was used for the construction of the PH and CHU extraction method. Experiment 2 was used for the validation of the method in 2023. And Experiments 1, 2, and 3 were used to construct the optimal AGB inversion model using a total of 136 experimental plots, measured AGB at four fertility periods, to form a measured dataset of 544 data points, combined with SPs parameters extracted from point cloud data to construct the optimal AGB inversion model.

Experiment 1 was conducted in 2022 at the Maize Center Research Base of the Beijing Academy of Agricultural and Forestry Sciences (BAFS), Tongzhou District, Beijing, China ($40^{\circ}35'N$, $117^{\circ}19'E$). The experimental region was a long-term localized N fertilization gradient trial plot of approximately 0.4 ha. Ten maize cultivars were planted under seven N fertilizer gradients in Experiment 1 (Table 2), with a planting density of 60,000 plants/ha. The pure N application rates of this experiment were N0(0), N1(75 kg/ha), N2(150 kg/ha), N3(225 kg/ha), N4(300 kg/ha), N5(375 kg/ha), N6(450 kg/ha), and the fertilization method was half of bottom fertilizer and half of follow up fertilizer (uniform follow up fertilizer at the pulling stage). Due to the limitations of the area, except for the JKQZ516 cultivar, which was planted in an area of $3.6\text{ m} \times 5\text{ m}$ (6 rows), the other cultivars were planted in an area of $7.2\text{ m} \times 5\text{ m}$ (12 rows), with a total of 70 experimental plots; the specific distribution of the experimental site is shown in Figure 1a.

Experiment 2 was conducted in 2023 at the Inner Mongolia Agricultural University Vocational and Technical College ($40^{\circ}33'N$, $110^{\circ}31'E$), China. Maize plants were sown on April 30, containing three cultivars under six water treatment gradients: W0 (0), W1 ($600\text{ m}^3/\text{ha}$), W2 ($1200\text{ m}^3/\text{ha}$), W3 ($1800\text{ m}^3/\text{ha}$), W4 ($2400\text{ m}^3/\text{ha}$), and W5 ($3000\text{ m}^3/\text{ha}$). The plot size was $18\text{ m} \times 5.4\text{ m}$ (nine rows).

Experiment 3 was conducted in 2023 in the same region as Experiment 2. It consisted of 24 maize cultivars under normal (W180) and halved normal (W90) irrigation (Figure 1) with irrigation rates of $2700\text{ m}^3/\text{ha}$ and $1350\text{ m}^3/\text{ha}$, respectively. Each plot measured $5\text{ m} \times 5.4\text{ m}$ (nine rows). A total of 66 experimental plots were planted at a density of 67,500 plants/ha by 2023 (Figure 1b). Shallow buried drip irrigation was applied in six equal doses after maize sowing and during the key growth stages.

2.2. Data Acquisition and pre-processing

2.2.1. UAV data acquisition

The CropLidar UAV phenotyping platform was used for data acquisition with a Matrix M300 RTK UAV as the sensor-mounting platform (DJI Inc., Guangdong, China). The positioning accuracy was enhanced using a ground-based RTK-GNSS base station (real-time kinematic-global navigation satellite system) (Figure 1c). A 3D lidar (Livox Avia,

Table 1
Details of the three experiments conducted in 2022 and 2023

Experimental	1	2	3
Year	2022	2023	2023
Number of cultivars	10	3	24
Number of treatments	7	6	2
Number of plots	70	18	48
Number of plants in plots	6 rows: 100 12 rows: 200	648	180
Spacing	$0.6 \times 0.3\text{ m}$	$0.6 \times 0.25\text{ m}$	$0.6 \times 0.25\text{ m}$

Table 2
Cross-reference table for cultivar

Year	Cultivar ID	Cultivar Name	Abbreviation
2022	C1	Jingkeqingzu-516	JKQZ516
	C2	Dika-159	DK159
	C3	Liangyu-99	LY99
	C4	Zhengdan-958	ZD958
	C5	Xianyu-335	XY335
	C6	MC-121	MC121
	C7	Jingnongke-728	JNK728
	C8	MC-812	MC812
	C9	Jingnongke-828	JNK828
	C10	Jingke-999	JK999
	C11	MC-121	MC121
	C12	Jingke-968	JK968
	C13	Dika-159	DK159
2023			

Note: The cultivars grown in experiment 1 were C1-C10, while the cultivars grown in the first part of experiment 2 were C11-C13. MC121 and DK159 appeared in both years of the experiment and were named C11 and C13, respectively, to differentiate between the different management practices. The names of the cultivars used in Experiment 3 are listed in Supplementary Table S1.

Shenzhen, China), GNSS satellite positioning system (UB4B0M, Beijing, China), and inertial navigation system (IMUMG-107E, Anhui, China) were used for the radar scanning system, with specific parameters listed in Table 3. This study utilized waypoint flight planning to obtain precise 3D point-cloud data for plant canopies. The flight band for point cloud overlap was set at 85%, the flight altitude was 30 m, and the flight was speed 1 m/s (Figure 1a), and at this operating altitude, the laser ranging random error was less than 2 cm. A DJI GS Pro was used to plan the routes and set the mission parameters. In waypoint flight mode, the vehicle executed a maneuver of flying around the waypoint without passing it, and the turning radius for this maneuver was 4 m.

2.2.2. Measured data acquisition

To ensure data consistency, the ground measurements and UAV flights were performed on the same day. Crop height was measured in the field using a ruler from the soil surface to the crop apex. Plant height was measured as the vertical height from the plant apex to the ground surface (Figure 1d) and we employed two measurement strategy: pre-tasseling, when the apex was the highest point of the plant in the vertical direction, the highest point of the plant leaves was used as the plant height, whereas post-tasseling, when the apex of the plant was the male spike, the vertical height of the male spike from the ground was measured (Xie et al., 2021). Ten plants were selected randomly from each plot. Average plant height was defined as the canopy height of the plot. During the key growth stages, we measured the aboveground dry biomass by selecting three maize plants with uniform growth status in each plot. The aboveground parts were dried in an oven at 80°C until they reached a constant weight. The AGB of maize in each experimental plot was calculated based on planted area and density. The intervals between fertility periods found to show a slight variation between years, which reflects the fact that Experiment 1 was conducted on summer maize with a fertility period of approximately 120 days, whereas Experiments 2 and 3 were conducted on spring maize with a fertility period of approximately 150 days. Table 4 presents details of the time and corresponding growth stages of data acquisition (Ciampitti et al., 2011).

2.2.3. Lidar data pre-processing

gAirHawk software was used to process the UAV data (Figure 2). This software generates a 3D point cloud using ground-based GNSS geospatial references from lidar files (.lid files), and INS data (.dat files) acquired using a UAV. Data were corrected to WG84 using a Gaussian (Transverse Mercator) projection and a 117° (Tongzhou District, Beijing, China) central meridian. The resulting data were then stored in a .las file format for further parameter extraction.

2.3. Phenotypes extraction

2.3.1. Point cloud segmentation and individual plant height estimation.

We developed an automated maize population-plot-plant segmentation and plant height extraction algorithm using the following steps: point cloud denoising, down-sampling, vegetation and ground detection, canopy to plant point cloud segmentation, and plant height estimation. The algorithm first statistically denoised the point cloud data from the input lidar (`nb_neighbors=30, std_ratio=2.0`) and then down-sampled the voxels (`voxel_size=0.01`) to increase the processing efficiency. In this case, down-sampling is required due to the fact that aerial tape splicing increases the point cloud density, and it is desirable to keep the sampling distance smaller than the average point spacing (1 cm in this document). Ground and vegetation segmentation was performed by using the “Cloth Simulation Filtering Algorithm” (CSF, `bSloopSmooth = False`, `cloth_resolution = 0.1`, `rigidness = 2`, `time_step = 0.5`, `class_threshold = 0.08`, `iterations = 1.0`, and `voxel_size = 0.01`, `threshold = 0.08`, number of iterations = 500).

After removing the ground, ground and vegetation segmentation for each period was assessed, and points with elevation values greater than the mean were removed from each plot, which contributes to addressing the issue of situations in which some vegetation bases are incorrectly classified as ground when fully covered by vegetation, due to the exposure of a smaller area of ground (Figure 3b). The point cloud of the maize population was then rotated so that the row direction was parallel to the Y-coordinate axis and the plots were segmented according to their length and width. Based on plot segmentation, the point cloud data of each plot was divided into rasters in the XY plane according to the actual planting row spacing. Each point cloud within a raster was considered to be an individual plant. Plant height of each individual was derived using the highest point height in each individual plant subtracts the mean value of the ground height (Figure 3). To eliminate the effect of missing plants due to field sampling on plant height extraction, we performed comparisons of the height of each single plant with the mean value of all plant heights in the plot. Plant height values that were lower than 1/2 of the mean value were automatically excluded.

2.3.2. Quantification of canopy height uniformity and marginal effects

The crop canopy height uniformity (CHU) (Eq. (1)) is quantified by the individual plant heights extracted from UAV remote sensing data. CHU is a measure of the uniformity of the crop canopy height. This describes the extent to which individual plants within a population deviate from the average plant height. The height uniformity of the crop population increased as the CHU increased and decreased as the CHU decreased, where $CV(PH)$ represents the coefficient of variation of individual plants within a population.

This study investigated the relationship between cultivation practices and CHU at different times, as well as the impact of canopy internal structure on CHU. The marginal effect ME_{PH} is defined as the uneven distribution of growth factors, such as fertilizer, water, and light, which may increase the height variation of plants in the side rows, particularly if the factor is initially insufficient. Plant height (PH) was calculated by defining the two lines of plants at the edge of the plot as the border. The mean value of a single plant height was extracted as $PH_{borderline}$, and the mean value of plant height inside the plot was calculated as $PH_{internal}$ (Eq. (2)).

$$CHU = \frac{1}{CV(PH)} \# \quad (1)$$

$$ME_{PH} = PH_{borderline} - PH_{internal} \# \quad (2)$$

2.4. AGB Estimation Models

A statistical multiple linear regression (MLR) model and three commonly used machine learning (ML) methods, random forest (RF),

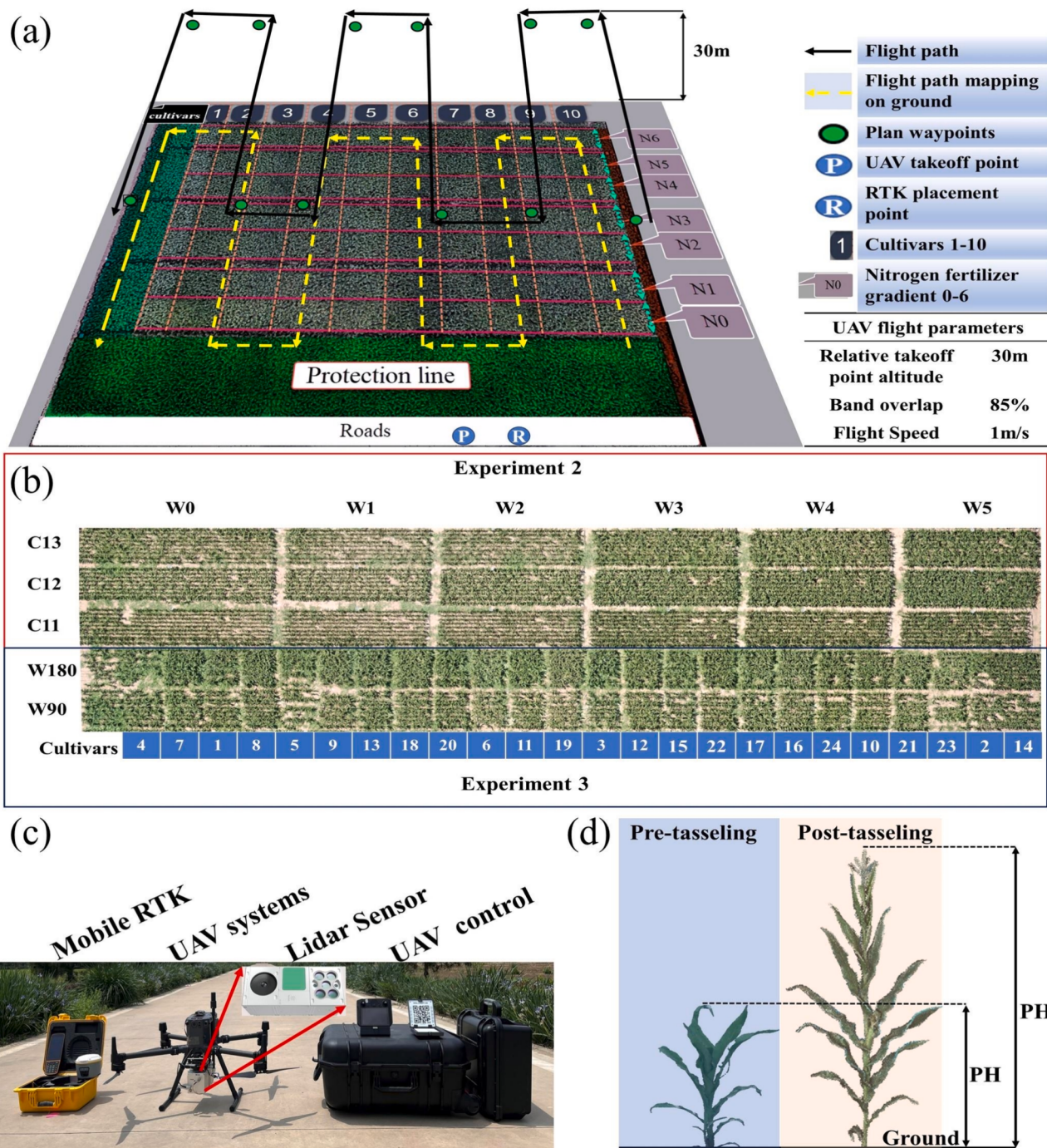


Figure 1. Experimental design and data acquisition equipment. (a) the 2022 experimental design and flight parameter settings, (b) the 2023 experimental design, (c) phenotyping platform composition, and (d) a schematic diagram of the different strategies employed for measuring plant height.

Table 3
Lidar sensor parameters in CropLidar UAV platform.

Lidar parameters	system parameter
Distance measurement	190 meters-10 % reflectivity; 260 meters-20 % reflectivity; 450 meters-80 % reflectivity;
Laser lines	Equivalent 64 lines
Ranging accuracy	1σ (@ 30 m) < 2 cm
Data volume	Three echoes, 720,000 points/second.
Field of view	70°

extreme gradient boosting (XGBOOST), and support vector machine (SVM), were used. This study combined these methods with a hyperparameter optimization algorithm to identify the best hyperparameter combinations. Canopy SP parameters were extracted from a point cloud of maize canopies removed from the ground (Table 5). The specific calculations of SPs are presented in Supplementary Table S2. The base dataset used in this study comprised the SPs parameters, which were gradually integrated into CHU and PH to estimate AGB.

The Pelican Optimization Algorithm (POA) is a heuristic search algorithm that simulates mechanisms found in nature, such as evolution and group behavior, to achieve global search capability and adaptivity. It intelligently searches the hyperparameter space and gradually

Table 4
Measured data information

Growth Stage	Description	Corresponding dates in 2022	Measurement in 2022		Corresponding dates in 2023	Measurement in 2023	
			PH	AGB		PH	AGB
V6	Sixth spreading leaf	July 16, 2022	✓	✓	June 15, 2023	✓	✓
V9	Ninth spreading leaf	July 24, 2022	✓	✓	June 30, 2023	✓	✓
V13	Thirteenth spreading leaf	July 29, 2022	✓	✓	July 15, 2023	✓	✓
VT	Tassel	August 13, 2022	✓	✓	July 24, 2023	✓	✓
R2	Silking	August 27, 2022	✓	✓	August 4, 2023	/	✓

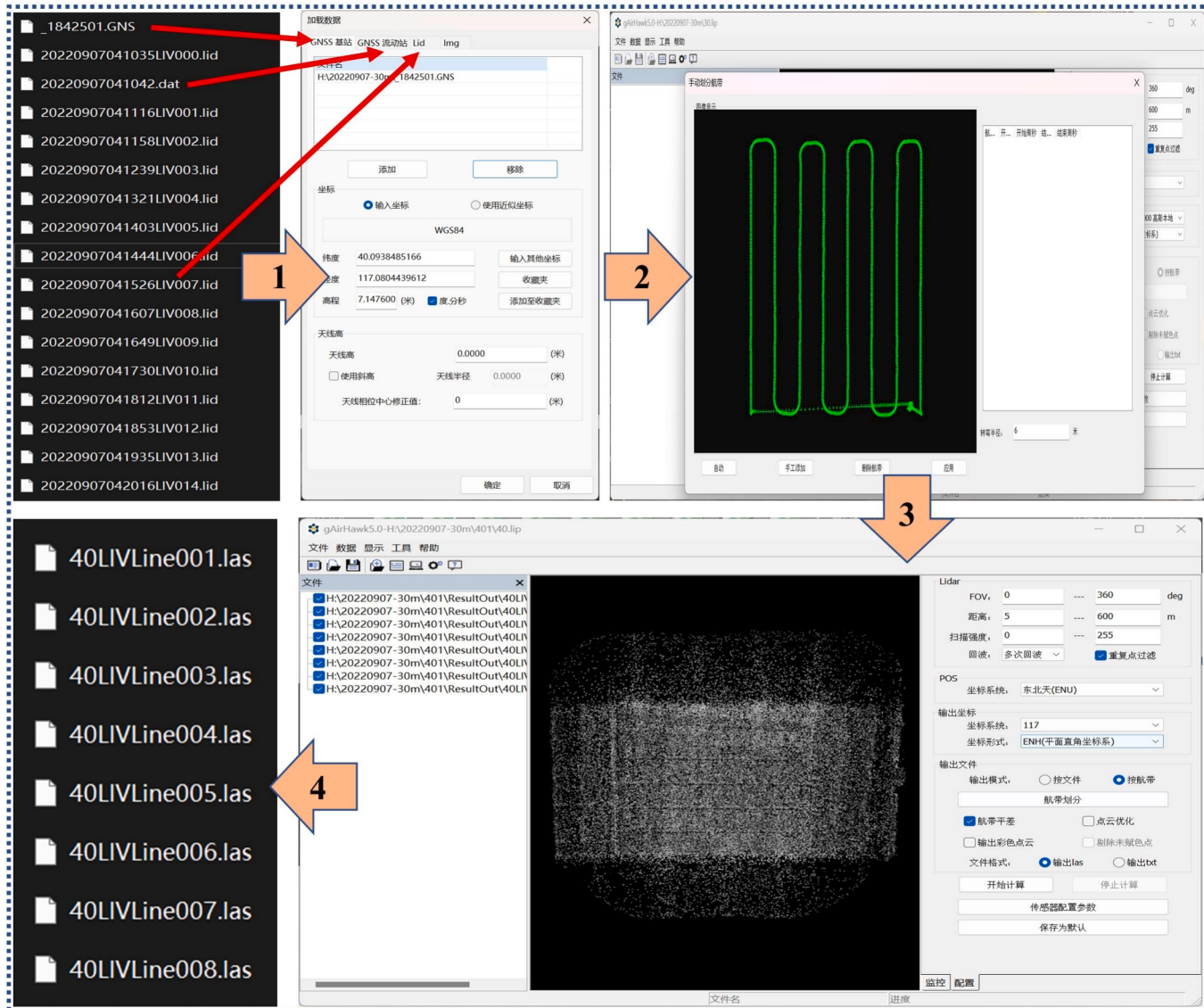


Figure 2. Flow for pre-processing point clouds

approximates the optimal solution during the search process, allowing it to find the optimal hyperparameter combinations (Trojovsky and Dehghani, 2022). Based on this algorithm, a process for optimizing the hyperparameters of machine models was developed (Figure 4). The iterative optimization process involved the following steps: (1) Selection: The parents who generated new individuals were selected based on their fitness values. (2) Mutation: Parents undergo mutation to generate new individuals. (3) Crossover: Parent individuals undergo crossover operations to generate new individuals. (4) Fitness Evaluation: The fitness values of the newly generated individuals should be evaluated.

The population should then be updated based on the set-selection strategy, retaining the individual with the smallest fitness value. The best hyperparameters and the individual with the smallest fitness value were output, representing the combination of hyperparameters at that point in time and using them to train the final model.

To train the model, the two-year datasets ($n=544$) from the two ecological sites were divided into training, validation, and test datasets. The datasets were divided based on the pre-tasseling (V6/V9, V13) and post-tasseling (VT, R2) and were randomized before training. We used an 8:1:1 ratio to divide the datasets into training, validation, and testing.

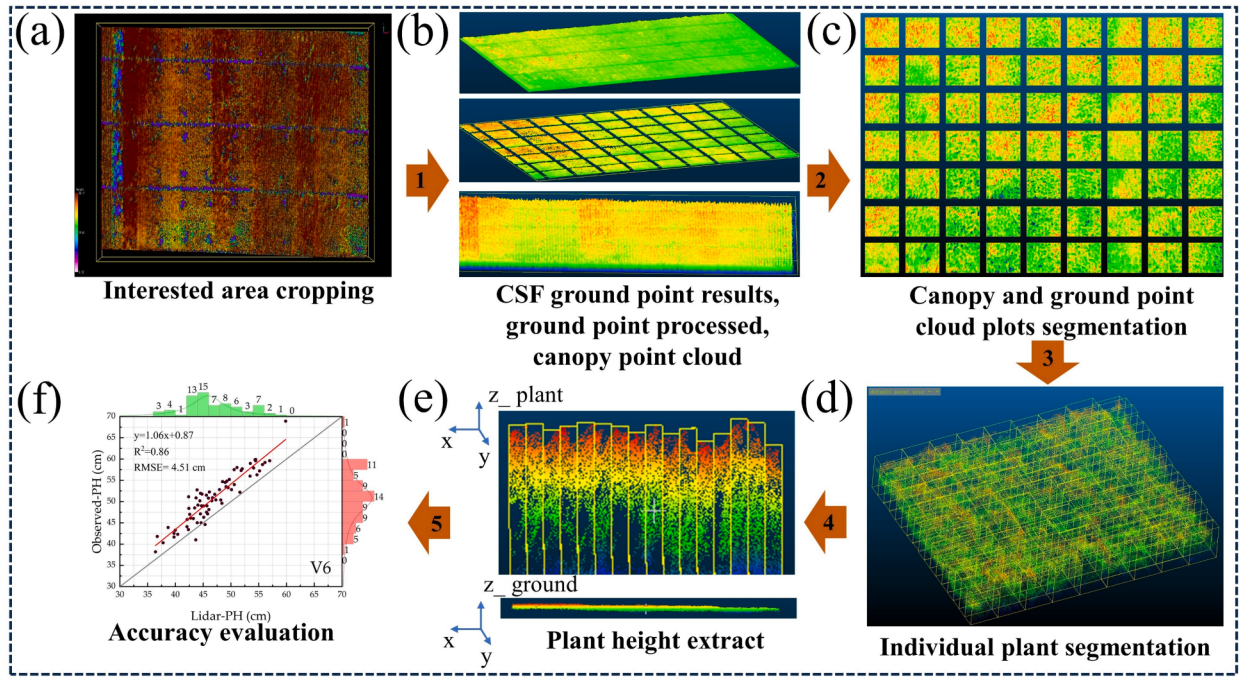


Figure 3. Point cloud segmentation and plant height estimation. (a) Cropping of the area of interest. (b) The point cloud of the ground before and after inspection of the ground during the R2 period, as well as the point cloud of the canopy, were created from the top to the bottom. (c) Canopy and ground point cloud plots segmentation. (d) Point cloud segmentation from plot to individual plants. (e) Plant height estimation using point clouds of individuals. (f) Plant height accuracy evaluation.

Table 5
Structural parameters used in the study

Parameter name	Descriptive	Parameter name	Descriptive
HStd	Heights standard deviation	HCover95	95 % height quartile coverage
HCV	Coefficient of variation of height	HCover90	90 % height quartile coverage
HCoverCV	Coefficient of Variation of Coverage	HCover75	75 % height quartile coverage
HCoverMean	Mean coverage value	HCover50	50 % height quartile coverage
HCoverStd	Standard deviation of coverage	Coverage75	Coverage at 75 % canopy height
H95	Canopy point cloud heights at the 95th percentile	Coverage50	Coverage at 50 % canopy height
H90	Canopy point cloud heights at the 90th percentile	Coverage25	Coverage at 25 % canopy height
H75	Canopy point cloud heights at the 75th percentile	Coverage0	Canopy coverage
H50	Canopy point cloud heights at the 50th percentile	Hmean	Mean canopy point cloud height

Assuming that the ML model is F_B and the hyperparameters are θ , the model is trained using the training data $(x'_\text{train}, y'_\text{train})$ and the hyperparameters. The trained model predicts the value of \hat{y}_valid , and the fitness function is calculated using Eqs. (3) - (5).

$$F_B = f(x'_\text{train}, y'_\text{train}, \theta) \# \quad (3)$$

$$\hat{y}_\text{valid} = F_B(x'_\text{valid}) \# \quad (4)$$

$$\text{fitness} = \frac{1}{N} \sum |\hat{y}_\text{valid} - y'_\text{valid}| \# \quad (5)$$

2.5. Evaluating indicators

To evaluate the accuracy of the estimated plant heights, Pearson's correlation coefficient and root-mean-square error (RMSE) were utilized. Additionally, the performance of the biomass estimation model was evaluated using the coefficient of determination (R^2) and relative root mean square error (rRMSE). Eq. (6-8) were used to calculate R^2 , RMSE, and rRMSE, where N represents the number of samples, i represents the sample index, y_i is the measured value, \hat{y}_i is the predicted value, and \bar{y}_i is the measured mean.

$$R^2 = 1 - \frac{\sum_{i=1}^N (y_i - \hat{y}_i)^2}{\sum_{i=1}^N (y_i - \bar{y}_i)^2} \# \quad (6)$$

$$\text{RMSE} = \sqrt{\frac{1}{N} \sum_{i=1}^N (y_i - \hat{y}_i)^2} \# \quad (7)$$

$$\text{rRMSE} = \frac{\sqrt{\frac{1}{N} \sum_{i=1}^N (y_i - \hat{y}_i)^2}}{\bar{y}} \times 100\% \# \quad (8)$$

3. Results

3.1. Evaluating the plant height accuracy of individuals in plots

Figures 5 and 6 illustrate the comparison of estimated and measured plant height for 2022 and 2023, respectively. The mean values of the individual plant heights extracted from all experimental plots were highly correlated with the averaging measured ones during the various growth stages. The results indicate that estimated plant height exhibited a strong correlation with measured plant height, with R^2 ranging from 0.85 to 0.93 across both years. The RMSE varied during different periods: starting at a minimum value of 4.51 cm (Figure 5a), peaking at a maximum of 12.56 cm (Figure 5b) as fertility progressed, and then slightly declining to 9.87 cm, with a smaller RMSE observed in the later

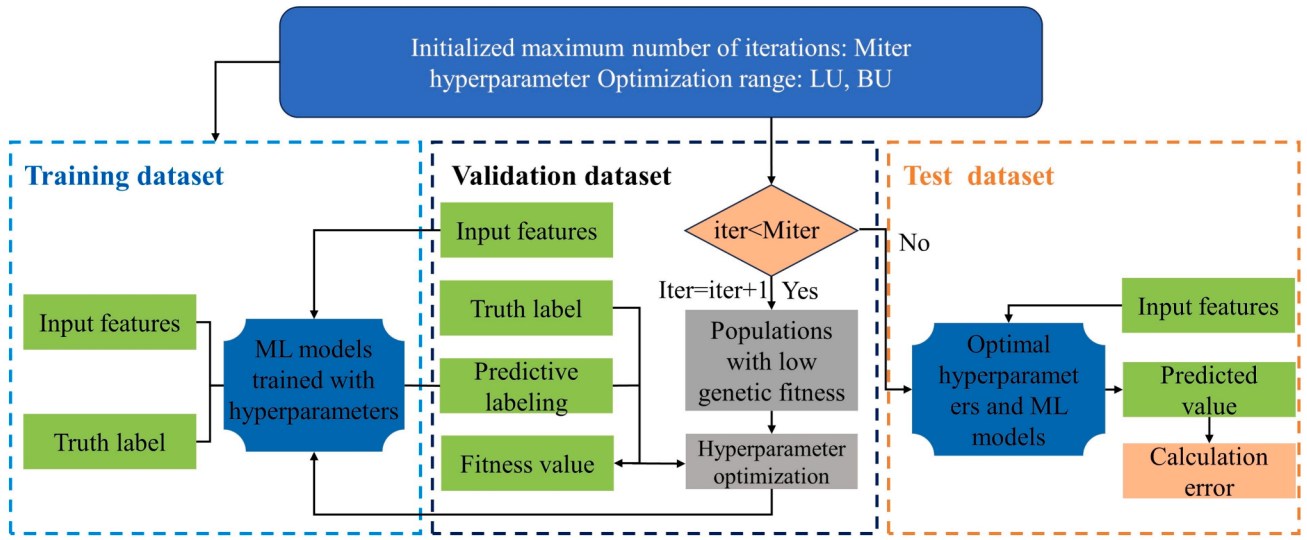


Figure 4. The model training process.

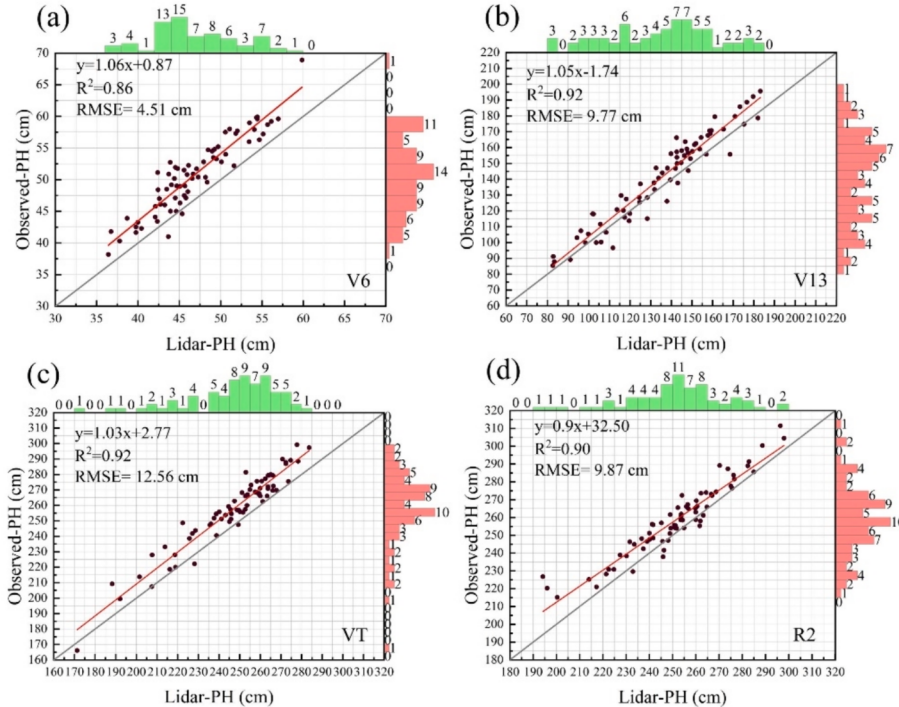


Figure 5. Validation of plant height accuracy in 2022. a-d shows the estimated and actual plant height for V6, V13, VT, and R2 periods.

period. Additionally, the validation results for plant height in 2023 showed stable extraction accuracy, with a difference of only 0.01 in R^2 and a reduction of 3.31 and 2.59 cm in RMSE compared to the 2022 V13 and VT periods. The experiment revealed differences in plant height estimation accuracy between different periods over the two years, with generally better accuracy in the pre-tasseling period than in the post-tasseling period.

3.2. Quantification of canopy structure of different cultivation practices using CHU

Based on the extracted individual plant heights, the CHU was calculated for different cultivation practices. Regarding to the N fertilizer application scenario (Experiment 1), Figure 7 illustrates the

variations in CHU for the ten maize cultivars in 2022. At the V6 growth stage, CHU in the N6 region with higher N fertilizer application was slightly higher than that in the other plots (Figure 7e). At this stage, cultivars showed no significant differences in CHU (Figure 7a). After the V6 fertilizer application, maize entered a rapid growth stage. At the V13 stage, an increase in N fertilizer application resulted in an increase in CHU (Figure 7b). For example, using the N2 treatment as a boundary, the CHU of maize populations above the N2 treatment ranged from 11.02 to 11.46, while those below the N2 treatment ranged from 6.89 to 8.93, and the lowest CHU was observed under the N0 treatment (Figure 7f). Interestingly, despite the gradual increase in N fertilizer application, CHU did not continue to increase but reached the maximum value under the N3 treatment (Figure 7g, h). For the variations in CHU among cultivars under the same fertilization treatment, using the R2

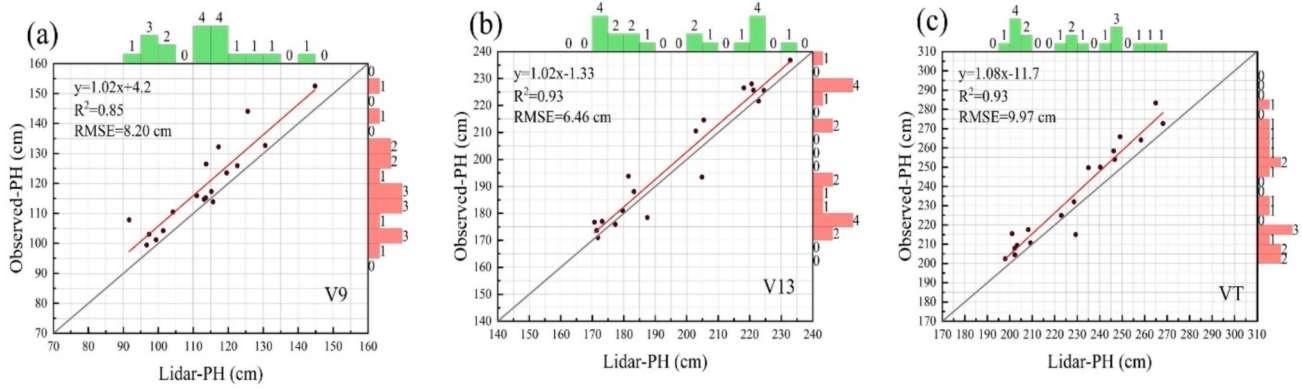


Figure 6. Validation of plant height accuracy in 2023. a-c shows the estimated and actual plant heights for V9, V13, and VT periods.

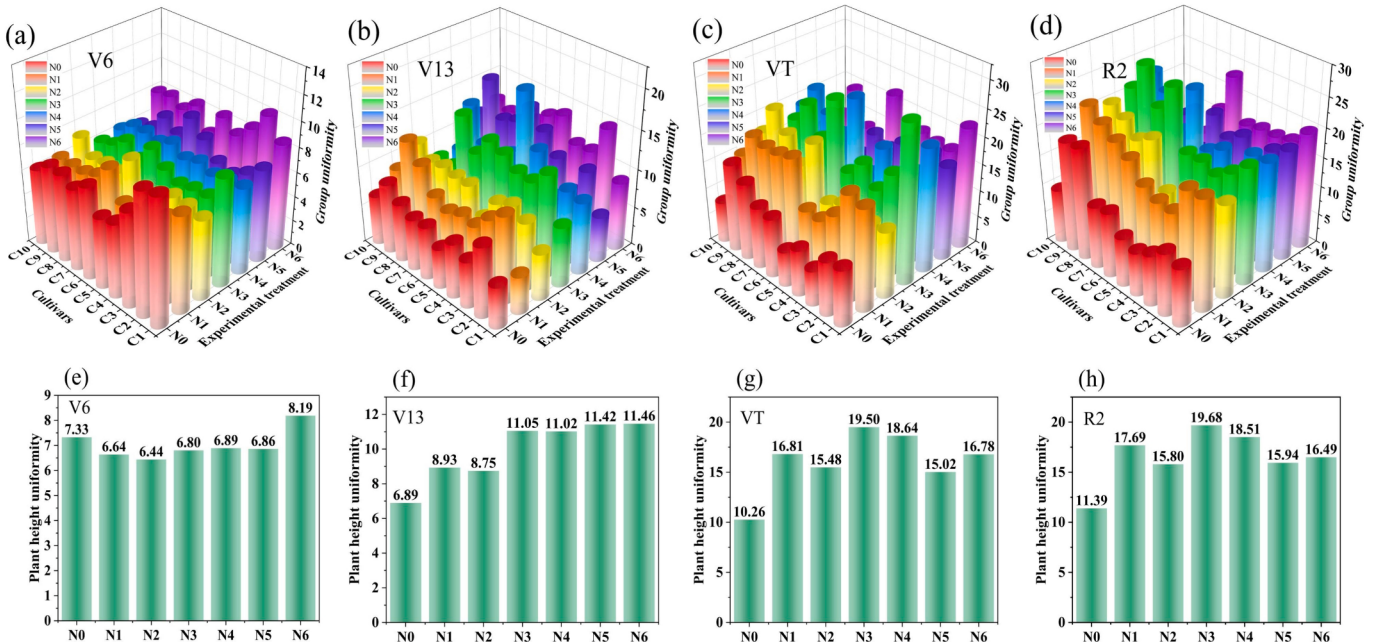


Figure 7. CHU variations among fertilizer treatments in 2022. a-d show the spatial distribution of cleanliness at different growth stages in 2022. e-f show the trends of different nitrogen fertilizer gradients at each stage.

period as an example, C8 (MC812) and C9 (JNK828) had higher CHU values than the other cultivars under the N0-N3 treatments, and they had a cleaner canopy structure than the other cultivars (Figure 7d). Increasing fertilizer application promoted higher CHU. When pure N was applied above 225 kg/ha (N3), the nutrient supply was sufficient, inter-individual differences in plant height increased, and CHU was slightly reduced.

Figure 8 shows the differences of CHU for cultivars under moisture gradients in Experiment 2 in 2023. CHU varied significantly among the treatments with increasing irrigation (Figure 8f-h), reaching its peak at the maximum irrigation W5, whereas the maximum value was achieved under the N3 treatment in the fertilizer scenario. Additionally, we found that moisture had a greater effect on CHU than nitrogen fertilizer treatments, and CHU was generally higher in the moisture treatments than in the nitrogen fertilizer treatments during the same period (Figure 7 f-h, Figure 8 f-h). These results emphasize that the CHU extracted in this study can effectively quantify the effects of the interaction between different management practices and cultivars and provide an effective quantitative assessment of canopy characteristics under different management conditions.

3.3. Evaluation the performance of CHU in AGB estimation

This study utilized multiple machine learning models, including MLR, POA-RF, POA-XGBOOST, and POA-SVM, to evaluate the effects of the CHU in AGB estimation during different stages of maize growth. The growth stage was divided into pre- and post-tasseling, and various data sources, such as SPs, PH, CHU, and combinations of these, were used (Table 6). The modeling results of the SPs dataset were compared, revealing that the gradual incorporation of the extracted PH and CHU into the data significantly improved the model estimation accuracy. During the pre-tasseling stages, the MLR, POA-RF, POA-XGBOOST, and POA-SVM methods achieved optimal R^2 values of 0.87, 0.88, 0.90, and 0.87, respectively, with rRMSE values of 40.09, 43.14, 37.68, and 43.44 %. The R^2 of the optimal model decreased during the post-tasseling stage. Specifically, the R^2 values of the four methods decreased by 0.17, 0.15, 0.04, and 0.17, whereas the rRMSE decreased by 9.14 %, 17.2 %, 23.9 %, and 17.78 %, respectively. The POA-XGBOOST model achieved the highest estimation accuracy among the different estimation methods on the other datasets, except for the pre-tasseling SPs+CHU dataset, for which the accuracy of the POA-SVM method was slightly higher than that of the POA-XGBOOST. According to the

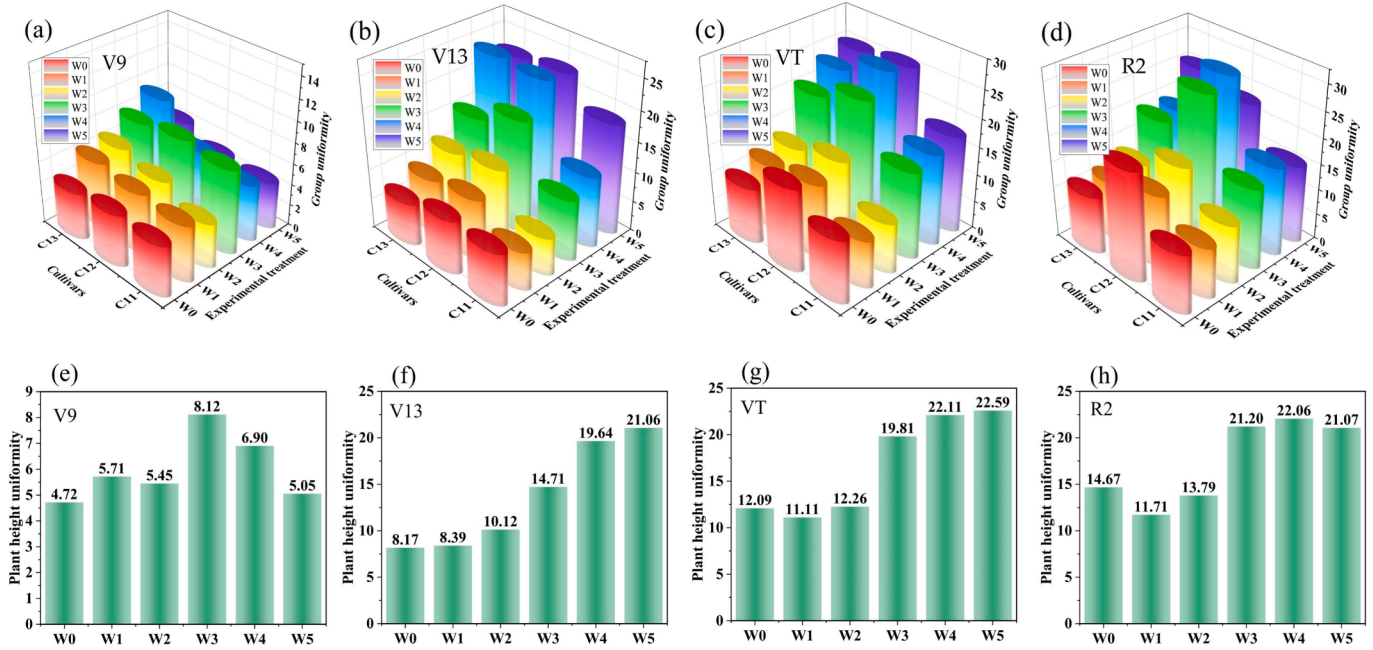


Figure 8. CHU variations among moisture treatments in 2023. a-d show the spatial distribution of cleanliness at different growth stages in 2023. e-f show the trends of different nitrogen fertilizer gradients at each period.

Table 6
AGB modeling results in different growth stages and datasets.

Growth stage	Features	MLR		POA-RF		POA-XGBOOST		POA-SVM	
		R ²	rRMSE(%)						
pre-tasseling	SPs	0.73	63.43	0.76	60.38	0.78	57.36	0.77	59.56
	SPs + PH	0.80	57.60	0.83	62.05	0.82	65.26	0.84	60.58
	SPs + CHU	0.78	50.10	0.87	47.21	0.90	41.95	0.83	53.43
	SPs + PH + CHU	0.87	40.09	0.88	43.14	0.90	37.68	0.87	43.44
post-tasseling	SPs	0.66	32.11	0.61	32.38	0.76	25.21	0.70	28.12
	SPs + PH	0.66	31.28	0.65	35.82	0.69	33.74	0.68	33.98
	SPs + CHU	0.67	26.56	0.67	24.58	0.79	25.77	0.64	25.47
	SPs + PH + CHU	0.70	30.95	0.73	25.94	0.86	13.78	0.70	25.66

statistical results, the POA-XGBOOST method demonstrated the highest estimation accuracy during both growth stages. The POA-SVM and POA-RF methods showed similar accuracy, while the MLR method was the least accurate (Figure 9). Those findings demonstrate the significance of CHU as a novel phenotypic indicator for AGB estimation. The CHU could effectively improve the model's estimation accuracy of AGB under

different water and fertilizer conditions.

3.4. Correlation analysis between CHU, SPs and AGB

Figure 10 shows a heat map of the correlation coefficients between the extracted CHU, SPs, and AGB in 2022 and 2023. The correlations

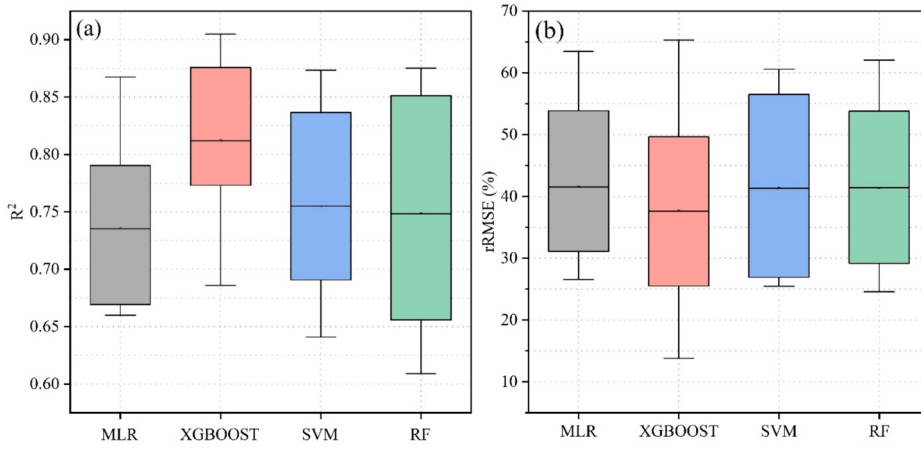


Figure 9. AGB estimation accuracy using different algorithms. (a) R², (b) rRMSE.

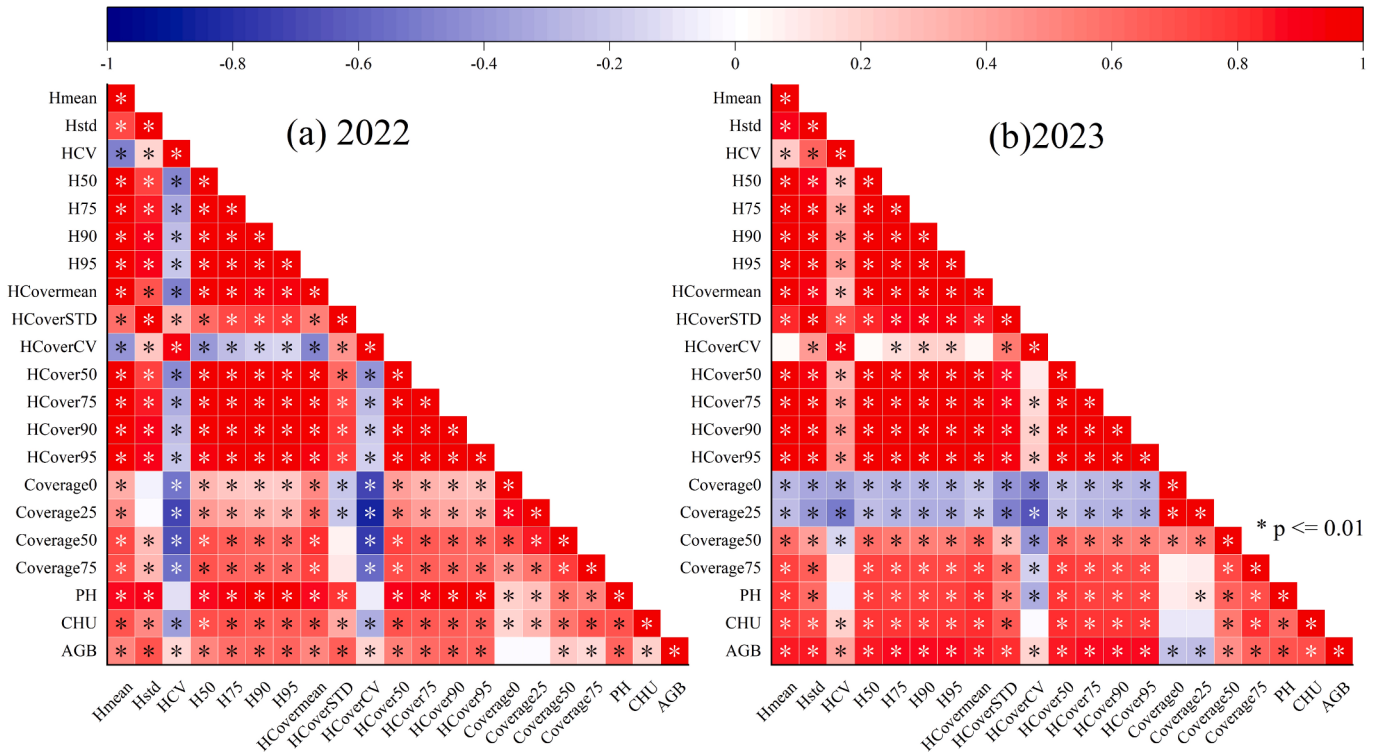


Figure 10. Correlation between CHU, SPs, and AGB.

among the indicators were consistent across both years. Significantly, a positive correlation between SPs and AGB was observed, indicating a close relationship with a high level of feature consistency. Additionally, CHU positively correlated with both PH and AGB. It also showed a correlation with SPs indicators, indicating that CHU is a phenotypic indicator that is closely related to canopy structure and AGB. Notably, HCV, HCoverCV, Coverage0, and Coverage25 showed weak positive or negative correlations with other indicators. This study found a strong positive correlation between the extracted SPs and AGB, as well as between PH and AGB, which is consistent with previous research (Wang et al., 2017; Shu et al., 2023). This relationship between AGB, SPs, and CHU is suitable for modeling and inverse mechanism interpretation.

3.5. Evaluating CHU and marginal effects in maize canopies

Figures 11-13 display the differences in canopy point clouds and marginal effects of the C12 cultivar in the 2023 moisture treatments in

V9, VT, and R2 stages. From the point cloud visualization, CHU can effectively characterize the canopy uniformities. During the V6 period, only minor differences in the CHU between treatments were observed. However, with persistent and continuous moisture deficits during the VT period, the CHU gradually increased as the volume of irrigation water increased. The highest CHU 26.63 was observed in W4 treatment, while the lowest was 13.18 in W1 treatment. During the R2 period, the CHU varied slightly among the moisture treatments. However, the basic trend remained the same as that during the VT period.

Figures 11-13g display the statistical results of side-row effects using side-row plant height versus internal plant height. The data indicate that the marginal effects become more pronounced as the maize growth (Figures 11-13g). The ME_{PH} in treatments W0-W5 were 0.04, -7.51, -5.37, -9.69, -0.02, and -3.07 cm, respectively. Additionally, the internal plant heights of the canopy were higher than that of the side rows in the V6 period. The plant heights of the side rows gradually exceeded that of the internal plants due to advancements in resources. During the VT

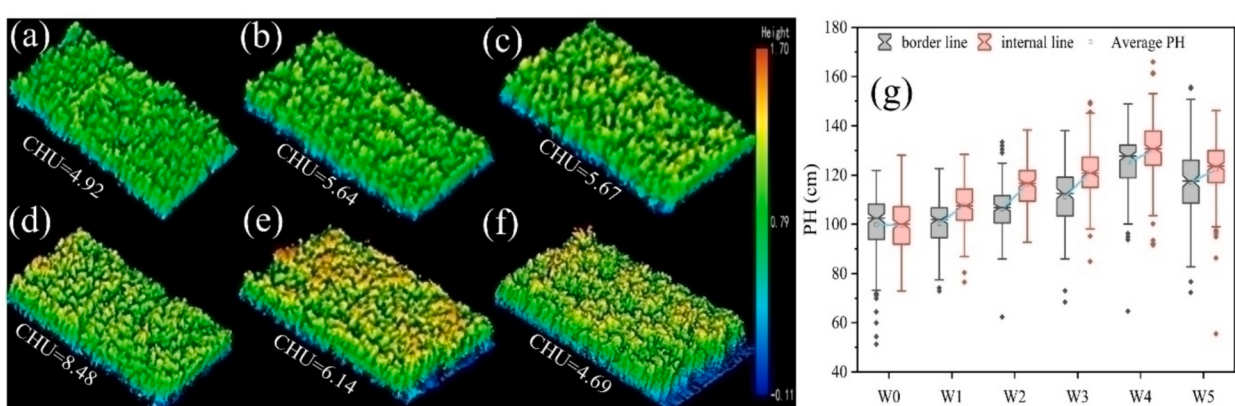


Figure 11. Canopy point cloud visualization corresponding and CHU results for treatments W0-W5 (a-f) of the V6 period of the C12 variety in 2023. Additionally, g shows the side-row effect, with the green line representing the average plant height.

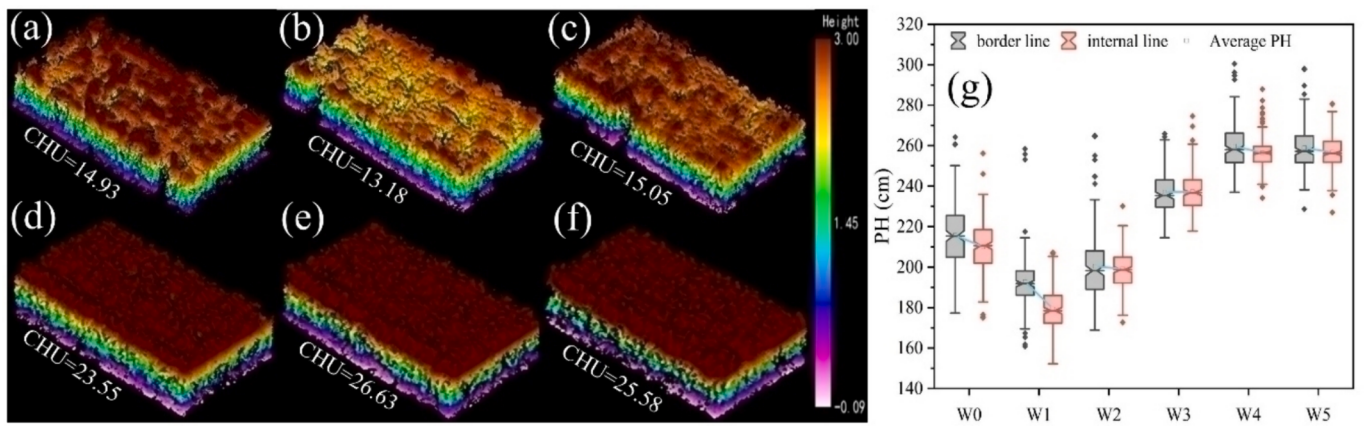


Figure 12. Canopy point cloud visualization corresponding and CHU results for treatments W0-W5 (a-f) of the VT period of the C12 variety in 2023. Additionally, g shows the side-row effect, with the green line representing the average plant height.

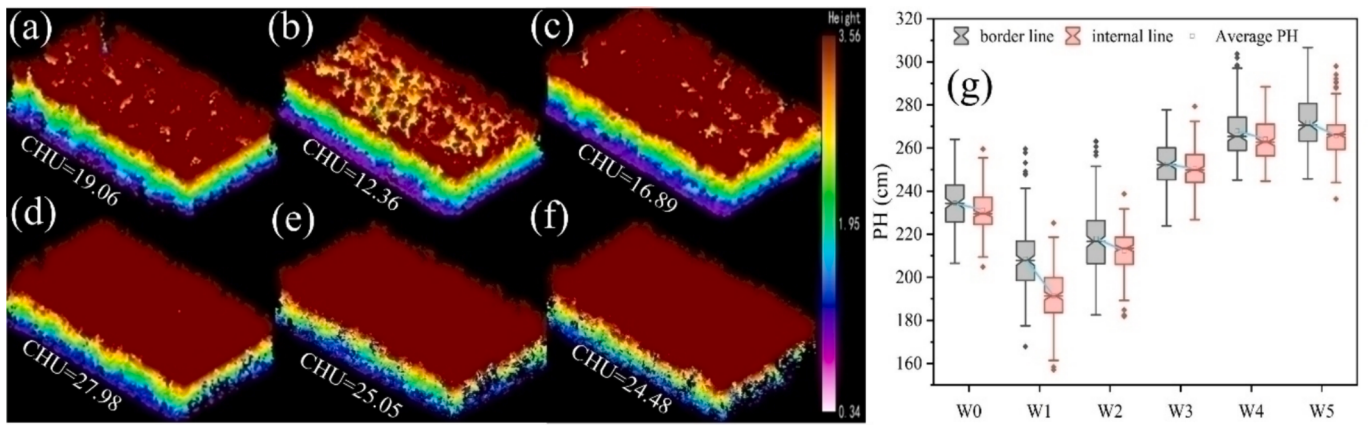


Figure 13. Canopy point cloud visualization corresponding and CHU results for treatments W0-W5 (a-f) of the R2 period of the C12 variety in 2023. Additionally, g shows the side-row effect, with the green line representing the average plant height.

period, the ME_{PH} of W0-W5 treatments were 5.59, 13.36, 1.35, -0.32, 3.12, and 2.14 cm. The maximum difference in ME_{PH} during the R2 period was 17.11 cm, with differences of 3.12, 6.35, 2.20, 3.60, and 6.20 cm. The CHU of W1 treatment was observed to be lower than that of W0 treatment, while the ME_{PH} was higher than that of W0 treatment. This difference may be attributed to the location of the W0 treatment at the edge of the experimental area, which resulted in additional water supplementation due to the leakage of the drip irrigation belt. Increasing the irrigation volume can alleviate the marginal effect and promote an increase in CHU, thereby promoting equal distribution of resources within the population.

4. Discussion

4.1. Crop height estimation based on UAV lidar: method strategy and error analysis

This study presents a method for plant height and CHU quantification that addresses the challenge of segmenting individual plants from maize canopies. The method combines the point cloud of the canopy population with row spacing and planting distances to achieve individual plant segmentation. Canopy height was calculated from the extracted heights of individual plants, considering the height variations of all plants within the canopy. In a recent study, Liu et al. used a plant height extraction method similarly. However, the lower boundaries were determined by the elevation values of the 1st and 5th quartiles, whereas the upper boundaries were determined by the heights of the

90th-100th quartiles. The method considers the ground and top of the crop as a 'neat plane' when correlating the measured PH (Liu et al., 2024). When the ground beneath the vegetation undulates or when there is increased competition for water and fertilizer among plants in the population, plant height varies greatly. For instance, when canopy structure is present, as depicted in Figure 13b, the height percentile may not accurately represent the population height. This limits the methodological applicability of using the height percentile method to estimate plant height.

The proposed method in this study considers the ground factor and the height differences among plants. It utilizes the difference between the elevation at the highest point of a single plant and the corresponding ground elevation as plant height. The method achieved a stable estimation accuracy in trials of cultivation practices in different ecological regions. The error was the greatest during the tasseling stage, and the estimated values were generally lower than the measured values, consistent with previous findings (Niu et al., 2019; Walter et al., 2019), as lidar sensors require a specific reflective area for detection. The proposed method for extracting plant height, as presented in this study, considers the impact of terrain on the estimation of plant height (Figure 3c). Furthermore, our findings indicated that the lidar estimation of plant height was consistently lower than the actual measurements (Figures 5 and 6) (Oehme et al., 2022; Liu et al., 2024). We speculate that this discrepancy may be attributable to the fact that the lidar sensor requires a specific reflective area for detection. The reflective area of the male spikes was found to be smaller when the UAV-acquired data was in the vertical direction. However, in the latter

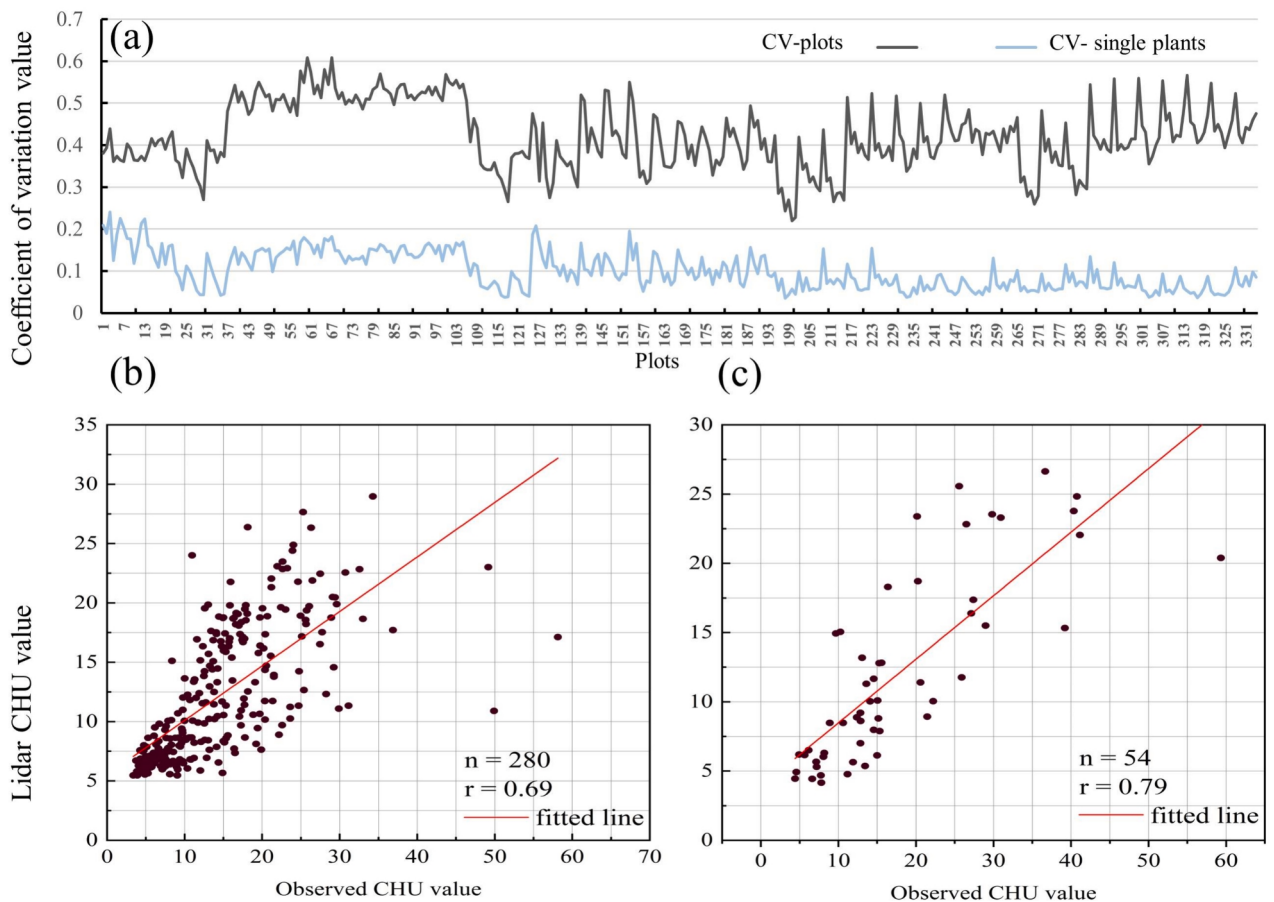


Figure 14. CHU reliability analysis. (a) Trends in the coefficient of variation of elevation and plant height within plots. (b) Correlation between CHU calculated based on manual measurements of plant height and CHU calculated using lidar.

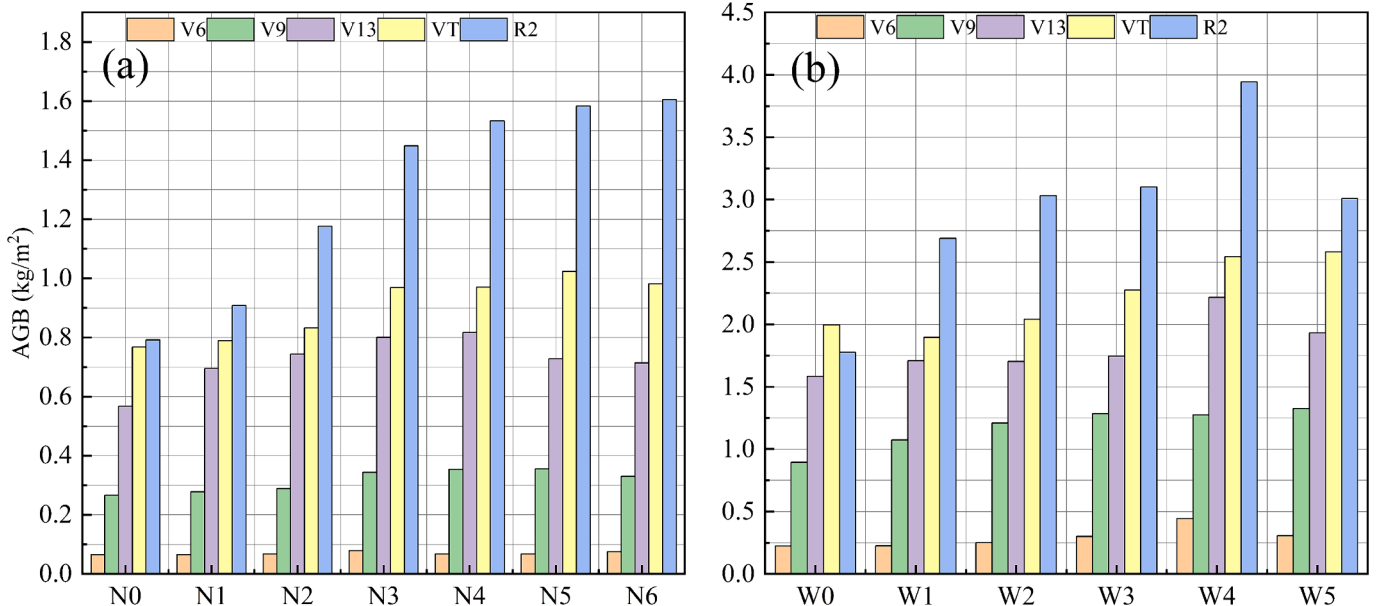


Figure 15. Change in AGB in response to irrigation and fertilization measures. (a) Example of the DK159 cultivar under nitrogen fertilizer gradient treatment in 2022. (b) Example of DK159 under an irrigation gradient in 2023.

stages of reproduction, the male spikes bend and complete pollen dispersal, resulting in an increase in the reflective area. Consequently, this enhanced the precision of plant height estimation. Concurrently,

our findings indicated that measures of water variability, and particularly the absence of nitrogen fertilization, resulted in a lower CHU (Figure 7f). This indicates that there is a high degree of variation in

individual plant heights within the population. Furthermore, the plants selected for artificial plant height measurements may not be sufficiently representative of the population as a whole. However, it is not practically feasible to measure the heights of all plants, which may have contributed to the discrepancy between the estimated and actual heights of plants.

4.2. Analysis of the role of CHU and its efficacy

The CHU is a phenotypic trait that connects individual plants to canopy. It is used to characterize the variability in plant height within a canopy. The CHU, calculated based on the extracted plant height of individual plants, enables the quantification of the canopy structure of different cultivation practices and cultivar interaction effects. Assessing the population structure is crucial in field production as it determines the efficiency of resource utilization (Liu et al., 2019; Liu et al., 2020). Furthermore, quantifying the high degree of interplant heterogeneity is important for the estimation of light distribution within plant canopy (Li et al., 2023). Shirzadifar et al. focused on seedling emergence uniformity and used the K-means clustering method with RGB images to assess the maize seedling emergence rate (Shirzadifar et al., 2020). Tian et al. also investigated the effect of sowing rate on cotton seedling emergence uniformity using image and deep learning methods (Tian et al., 2024). Canopy roughness metrics were utilized to estimate crop AGB. The RGB images acquired by the UAVs were used to create a canopy point cloud. Canopy roughness was then calculated to quantify canopy structure changes in different genotypes of soybeans (Herrero-Huerta et al., 2020). However, these methods may not be applicable to populations with high plant height variance, such as stressed maize populations. The effect of each maize plant on the population structure should be considered when quantifying the canopy structure. This study found that various cultivation practices significantly influenced CHU, which remained consistent during the periods of plant morphological stabilization (VT and R2). Moreover, although continuously increasing the amount of nitrogen fertilizer was effective in promoting an increase in plant height, it did not consistently enhance CHU (Figure 7). In the experiment with varying amounts of irrigation, there was a consistent increase in the CHU (Figure 8). Moreover, our experimental results clearly demonstrate the benefits of individual plant segmentation for extracting plant height, which allowed for the assessment of marginal effects in crop canopies. Marginal effects were observed in response to the fertility and irrigation treatments (Figure 13e). The validity of this index in evaluating canopy structure was demonstrated by CHU's effective quantification of treatment differences in various ecological regions and cultivation practices over two years.

The coefficient of variation of plant height, which is an important parameter for CHU calculation, indicates the degree of plant variation within a plot. In the 2-year experiments (Experiments 1 and 2), the trends in the coefficient of variation of point cloud elevation and the coefficient of variation calculated from plant height for a total of 334 plots were generally consistent (Figure 14a). Furthermore, the correlation between the CHU calculated from the manually measured plant heights within each plot and those calculated from the corresponding plots were found to be satisfactory (Figure 14b, c), despite the limited number of samples measured manually in each plot. These findings indicate that the proposed CHU can effectively reflect the population height variability characteristics.

4.3. The utility of SPs in AGB estimation

Images, point clouds, and spectra are crucial sources of phenotypic data for precision agriculture. Metrics such as vegetation indices, texture metrics, plant height, and cover extracted from multispectral and RGB images are widely used to estimate AGB (Yue et al., 2018). As mentioned in the literature review, the saturation of spectral data in the later stages of crop fertility limits the ability to estimate the AGB (Luo et al., 2017;

Swoish et al., 2022). To overcome the limitations of 2D spectral data, an increasing number of studies have integrated 3D information into AGB estimation studies for crops such as maize (Zhu et al., 2019), wheat (Song and Wang, 2019), and rice (Cen et al., 2019). In contrast to vegetation indices derived from spectral data, lidar data still rely on conventional metrics, such as crop height (Sun et al., 2017; Jin et al., 2018b) and canopy volume (Jin et al., 2018a). To enhance the use of lidar data for phenotypic resolution, this study utilized height, coverage, height quartile coverage, and coefficients of variation and standard deviation variables extracted from the point cloud data to form SPs for further analysis (Table 5).

The results of the correlation analysis demonstrated a statistically correlation between the majority of the SPs and AGB in the two-year trial (Figure 10). However, the correlation between CHU and AGB was not entirely consistent throughout the two-year trial, which may be attributed to the varying effects of water and fertilization measures on AGB and CHU. The trends of CHU and AGB of Trial 1 in different growth stages revealed slight discrepancies. AGB exhibited a gradual increase with increasing fertilizer application (Figure 15a), while CHU demonstrated a trend of initial increase followed by a decline during the VT and R2 stages (Figure 7e-h). The trends of CHU and AGB exhibited greater similarity in Trial 2, with both CHU and AGB demonstrating an upward trajectory with increasing irrigation (Figure 8e-h). Additionally, both R2 stages exhibited a slight decline following the highest point reached in the W4 treatment (Figure 15b). These results indicate that while increased nitrogen fertilizer application is conducive to AGB growth, high nitrogen fertilizer application is not conducive to a homogeneous population structure. However, increasing the irrigation volume in a coordinated manner would promote increases in CHU and AGB, with the objective of achieving a more homogeneous canopy structure, which resulted in a higher correlation between AGB and CHU in 2023 compared to 2022.

Machine learning algorithms can improve the accuracy of crop parameter estimations. This study compared two integrated learning models, POA-XGBOOST and POA-RF, to the POA-SVM method and found that the former two achieved better estimation results. This is because each base learner in the integrated learning has a different assumption space. Integrating these base learners expands the assumption space and improves the robustness of the integrated model for unknown distributed data (Zhai et al., 2023). Compared with the POA-XGBOOST method, the POA-RF method is less effective for estimation. This is likely due to XGBOOST's sensitivity of XGBOOST to hyperparameter selection, which requires more tuning to optimize the model performance. In contrast, RF is less sensitive to hyperparameter selection. XGBOOST integrates a regularization term that effectively controls the model complexity and reduces overfitting, unlike traditional gradient boosting algorithms (Sun et al., 2024). In addition, XGBOOST is optimized for managing sparse datasets, facilitating parallel computation, and supporting early stopping strategies, which improves training efficiency and model generalization. In this study, the Pelican Optimization Algorithm (POA)-based hyperparameter optimization algorithm was found to be effective in optimizing the XGBOOST method, resulting in optimal estimation results of POA-XGBOOST across different periods and datasets.

4.4. Limitations and future research directions

Although in this study we assessed the utility of the high-throughput estimation of CHU metrics for the first time and compared this with applications involving canopy description and AGB estimation, there remain a number interesting and important directions that warrant further investigation. In this study we based our analyses on regular planting planning, such as manually planning the plot size prior to planting and retaining standard corridors between plots, which may have led to the inapplicability of monoculture segmentation to irregular plots. Concurrently, there is a paucity of mature technical solutions for

the automatic identification and segmentation of plots based on point cloud data. In our projected future research, with the objective of enhancing the applicability of the method used in this study, we will endeavor to employ the method of multi-source data fusion, utilizing images for the identification and localization of monocultures and fusing point cloud 3D information for the automated identification and segmentation of monocultures.

5. Conclusions

This study explored the use of lidar data to extract individual plant heights by segmenting point clouds of maize canopies with a high accuracy. Additionally, the CHU was proposed as a new indicator to describe the height uniformity of plant canopy in a high-throughput manner using UAV platforms. CHU can rapidly screen for groups exhibiting high uniformity in terms of canopy structure quantification and is sensitive to responses to cultivation measures. When estimating AGB, the CHU accounted for the individual variability of the cultivation measures in the canopy. Among the four AGB modeling methods, the accuracies for estimating the models were ranked as follows: POA-XGBOOST > POA-SVM > POA-RF > MLR. POA-XGBOOST achieved excellent estimation accuracies at two growth stages and multiple dataset combinations, with optimal R² values at pre-tasseling and post-tasseling being 0.90 and 0.86, respectively. In summary, this study provides new indicator and technical supports for evaluating canopy structures.

CRediT authorship contribution statement

Wushuai Chang: Writing – review & editing, Writing – original draft, Methodology, Investigation, Formal analysis. **Weiliang Wen:** Writing – review & editing, Writing – original draft, Methodology, Conceptualization. **Shenghao Gu:** Visualization, Validation. **Yinglun Li:** Writing – review & editing, Formal analysis. **Jiangchuan Fan:** Software, Data curation. **Xianju Lu:** Resources. **Bo Chen:** Data curation. **Tianjun Xu:** Resources. **Ronghuan Wang:** Supervision. **Xinyu Guo:** Writing – review & editing, Supervision, Funding acquisition, Conceptualization. **Ruiqi Li:** Supervision, Project administration.

Declaration of competing interest

The authors declare that they have no known competing financial interests or personal relationships that could have appeared to influence the work reported in this paper.

Data availability

Data will be made available on request.

Acknowledgment

This work was partially supported by National Key R&D Program of China (2021YFD1200700), Science and Technology Innovation Special Construction Funded Program of Beijing Academy of Agriculture and Forestry Sciences (KJCX20220401), the National Natural Science Foundation of China (32071891), Reform and Development Project of Beijing Academy of Agriculture and Forestry Sciences, and the earmarked fund (CARS-02 and CARS-54).

Appendix A. Supplementary data

Supplementary data to this article can be found online at <https://doi.org/10.1016/j.compag.2024.109491>.

References

- Araza, A., De Bruin, S., Herold, M., Quegan, S., Labriere, N., et al., 2022. A comprehensive framework for assessing the accuracy and uncertainty of global above-ground biomass maps. *Remote Sensing of Environment* 272. <https://doi.org/10.1016/j.rse.2022.112917>.
- Bendig, J.V., 2015. Unmanned aerial vehicles (UAVs) for multi-temporal crop surface modelling. A new method for plant height and biomass estimation based on RGB-imaging. *Universität zu Köln*.
- Bendig, J., Yu, K., Asen, H., Bolten, A., Bennertz, S., et al., 2015. Combining UAV-based plant height from crop surface models, visible, and near infrared vegetation indices for biomass monitoring in barley. *International Journal of Applied Earth Observation and Geoinformation* 39, 79–87.
- Cen, H., Wan, L., Zhu, J., Li, Y., Li, X., et al., 2019. Dynamic monitoring of biomass of rice under different nitrogen treatments using a lightweight UAV with dual image-frame snapshot cameras. *Plant Methods* 15, 1–16.
- Ciampitti, I.A., Elmore, R.W., Lauer, J., 2011. Corn growth and development. Dent 5.
- Gilliot, J.M., Michelin, J., Hadjard, D., Houot, S., 2021. An accurate method for predicting spatial variability of maize yield from UAV-based plant height estimation: a tool for monitoring agronomic field experiments. *Precision Agriculture* 22, 897–921. <https://doi.org/10.1007/s11119-020-09764-w>.
- Has, V., Tokatlidis, I., Has, I., Mylonas, I., 2008. Optimum density and stand uniformity as determinant parameters of yield potential and productivity in early maize hybrids. *Romanian Agricultural Research* 25, 43–46.
- Herrero-Huerta, M., Bucksch, A., Puttemans, E., Rainey, K.M., 2020. Canopy roughness: A new phenotypic trait to estimate aboveground biomass from unmanned aerial system. *Plant Phenomics*.
- Huang, R., Li, G., 1995. Plant height consistencies in maize population and a comparison of their measuring techniques. *Journal of Maize Sciences* 3, 61–63.
- Jimenez-Berni, J.A., Deery, D.M., Rozas-Larraondo, P., Condon, A.G., Rebetzke, G.J., et al., 2018. High throughput determination of plant height, ground cover, and above-ground biomass in wheat with LiDAR. *Frontiers in Plant Science* 9. <https://doi.org/10.3389/fpls.2018.00237>.
- Jin, S., Su, Y., Gao, S., Wu, F., Hu, T., et al. (2018a). Deep learning: individual maize segmentation from terrestrial lidar data using faster R-CNN and regional growth algorithms. *Frontiers in plant science* 9, 866.
- Jin, S., Su, Y., Wu, F., Pang, S., Gao, S., et al. (2018b). Stem-leaf segmentation and phenotypic trait extraction of individual maize using terrestrial LiDAR data. *IEEE Transactions on Geoscience and Remote Sensing* 57, 1336–1346.
- Jin, S., Sun, X., Wu, F., Su, Y., Li, Y., et al., 2021. Lidar sheds new light on plant phenomics for plant breeding and management: Recent advances and future prospects. *Isprs Journal of Photogrammetry and Remote Sensing* 171, 202–223. <https://doi.org/10.1016/j.isprsjprs.2020.11.006>.
- Jin, X., Zarco-Tejada, P., Schmidhalter, U., Reynolds, M., Hawkesford, M., et al., 2020. High-throughput estimation of crop traits: a review of ground and aerial phenotyping platforms. *IEEE Geosci Remote Sens Mag*.
- Li, M., Hu, P., He, D., Zheng, B., Guo, Y., et al., 2023. Quantification of the Cumulative Shading Capacity in a Maize-Soybean Intercropping System Using an Unmanned Aerial Vehicle. *Plant Phenomics* 5, 0095.
- Li, B., Xu, X., Zhang, L., Han, J., Bian, C., et al., 2020. Above-ground biomass estimation and yield prediction in potato by using UAV-based RGB and hyperspectral imaging. *Isprs Journal of Photogrammetry and Remote Sensing* 162, 161–172. <https://doi.org/10.1016/j.isprsjprs.2020.02.013>.
- Liu, S., Martre, P., Buis, S., Abichou, M., Andrieu, B., et al., 2019. Estimation of plant and canopy architectural traits using the digital plant phenotyping platform. *Plant Physiology* 181, 881–890.
- Liu, G., Zhang, G., Hou, P., Liu, Y., Li, J., et al., 2020. Weak border effects and great uniformity increase yield of maize (*Zea mays*) under dense population. *Crop and Pasture Science* 71, 653–659.
- Liu, T., Zhu, S., Yang, T., Zhang, W., Xu, Y., et al., 2024. Maize height estimation using combined unmanned aerial vehicle oblique photography and LiDAR canopy dynamic characteristics. *Computers and Electronics in Agriculture* 218, 108685.
- Lu, Y., Zhang, X., Chen, S., Shao, L., Sun, H., et al., 2017. Increasing the planting uniformity improves the yield of summer maize. *Agronomy Journal* 109, 1463–1475. <https://doi.org/10.2134/agronj2016.12.0718>.
- Luo, S., Wang, C., Xi, X., Pan, F., Peng, D., et al., 2017. Fusion of airborne LiDAR data and hyperspectral imagery for aboveground and belowground forest biomass estimation. *Ecological Indicators* 73, 378–387. <https://doi.org/10.1016/j.ecolind.2016.10.001>.
- Madec, S., Baret, F., De Solan, B., Thomas, S., Dutartre, D., et al., 2017. High-throughput phenotyping of plant height: comparing unmanned aerial vehicles and ground LiDAR estimates. *Frontiers in plant science* 8, 2002.
- Niu, Y., Zhang, L., Zhang, H., Han, W., Peng, X., 2019. Estimating above-ground biomass of maize using features derived from UAV-based RGB imagery. *Remote Sensing* 11. <https://doi.org/10.3390/rs11111261>.
- Oehme, L.H., Reineke, A.-J., Weiß, T.M., Würschum, T., He, X., et al., 2022. Remote sensing of maize plant height at different growth stages using UAV-based digital surface models (DSM). *Agronomy* 12, 958.
- Prabhakara, K., Hively, W.D., McCarty, G.W., 2015. Evaluating the relationship between biomass, percent groundcover and remote sensing indices across six winter cover crop fields in Maryland, United States. *International Journal of Applied Earth Observation and Geoinformation* 39, 88–102. <https://doi.org/10.1016/j.jag.2015.03.002>.
- Shirzadifar, A., Maharloei, M., Bajwa, S.G., Oduor, P.G., Nowatzki, J.F., 2020. Mapping crop stand count and planting uniformity using high resolution imagery in a maize crop. *Biosystems Engineering* 200. <https://doi.org/10.1016/j.biosystemseng.2020.10.013>.

- Shu, M., Li, Q., Ghafoor, A., Zhu, J., Li, B., et al., 2023. Using the plant height and canopy coverage to estimation maize aboveground biomass with UAV digital images. *European Journal of Agronomy* 151, 126957.
- Song, Y., Wang, J., 2019. Winter wheat canopy height extraction from UAV-based point cloud data with a moving cuboid filter. *Remote Sensing* 11, 1239.
- Sun, S., Li, C., Paterson, A., 2017. In-field high-throughput phenotyping of cotton plant height using LiDAR. *Remote Sens* 9 (4).
- Sun, Z., Li, Y., Yang, Y., Su, L., Xie, S., 2024. Splitting tensile strength of basalt fiber reinforced coral aggregate concrete: Optimized XGBoost models and experimental validation. *Construction and Building Materials* 416, 135133.
- Swoish, M., Leme Filho, J.F.D.C., Reiter, M.S., Campbell, J.B., Thomason, W.E., 2022. Comparing satellites and vegetation indices for cover crop biomass estimation. *Computers and Electronics in Agriculture* 196. <https://doi.org/10.1016/j.compag.2022.106900>.
- Tian, F., Ransom, C.J., Zhou, J., Wilson, B., Sudduth, K.A., 2024. Assessing the impact of soil and field conditions on cotton crop emergence using UAV-based imagery. *Computers and Electronics in Agriculture* 218, 108738.
- Trojovský, P., Dehghani, M., 2022. Pelican optimization algorithm: A novel nature-inspired algorithm for engineering applications. *Sensors* 22, 855.
- Walter, J.D.C., Edwards, J., McDonald, G., Kuchel, H., 2019. Estimating biomass and canopy height With LiDAR for field crop breeding. *Frontiers in Plant Science* 10,1145. doi:10.3389/fpls.2019.01145.
- Wang, C., Nie, S., Xi, X., Luo, S., Sun, X., 2017. Estimating the biomass of maize with hyperspectral and LiDAR data. *Remote Sensing* 9,11. doi:10.3390/rs9010011.
- Wang, X., Zhang, R., Song, W., Han, L., Liu, X., et al., 2019. Dynamic plant height QTL revealed in maize through remote sensing phenotyping using a high-throughput unmanned aerial vehicle (UAV). *Scientific Reports* 9. <https://doi.org/10.1038/s41598-019-39448-z>.
- Wang, H., Zhang, W., Yang, G., Lei, L., Han, S., et al., 2023. Maize ear height and ear-plant height ratio estimation with LiDAR data and vertical leaf area profile. *Remote Sensing* 15. <https://doi.org/10.3390/rs15040964>.
- Xie, T., Li, J., Yang, C., Jiang, Z., Chen, Y., et al., 2021. Crop height estimation based on UAV images: Methods, errors, and strategies. *Computers and Electronics in Agriculture* 185. <https://doi.org/10.1016/j.compag.2021.106155>.
- Yuan, W., Li, J., Bhatta, M., Shi, Y., Baenziger, P.S., et al., 2018. Wheat height estimation using LiDAR in comparison to ultrasonic sensor and UAS. *Sensors* 18. <https://doi.org/10.3390/s18113731>.
- Yue, J., Feng, H., Jin, X., Yuan, H., Li, Z., et al., 2018. A comparison of crop parameters estimation using images from UAV-mounted snapshot hyperspectral sensor and high-definition digital camera. *Remote Sensing* 10, 1138.
- Yue, J., Yang, H., Yang, G., Fu, Y., Wang, H., et al., 2023. Estimating vertically growing crop above-ground biomass based on UAV remote sensing. *Computers and Electronics in Agriculture* 205. <https://doi.org/10.1016/j.compag.2023.107627>.
- Zhai, W., Li, C., Fei, S., Liu, Y., Ding, F., et al., 2023. CatBoost algorithm for estimating maize above-ground biomass using unmanned aerial vehicle-based multi-source sensor data and SPAD values. *Computers and Electronics in Agriculture* 214, 108306.
- Zhu, W., Sun, Z., Peng, J., Huang, Y., Li, J., et al., 2019. Estimating maize above-ground biomass using 3D point clouds of multi-source unmanned aerial vehicle data at multi-spatial scales. *Remote Sensing* 11, 2678.